Bull Mater Sci (2020) 43:249
https://doi.org/10.1007/s12034-020-02217-0

Fabrication and characterization of three-dimensional porous cornstarch/n-HAp biocomposite scaffold

C Y BEH[1], E M CHENG[1,*], N F MOHD NASIR[1], M S ABDUL MAJID[1], M R MOHD ROSLAN[1], K Y YOU[2], S F KHOR[3] and M J M RIDZUAN[1]

[1] School of Mechatronic Engineering, University Malaysia Perlis (UniMAP), Pauh Putra Campus, 02600 Arau, Perlis, Malaysia
[2] School of Electrical Engineering, Faculty of Engineering, Universiti Teknologi Malaysia, 81310 Skudai, Johor, Malaysia
[3] School of Electrical Systems Engineering, Universiti Malaysia Perlis (UniMAP), Pauh Putra Campus, 02600 Arau, Perlis, Malaysia
*Author for correspondence (emcheng@unimap.edu.my)

MS received 9 November 2019; accepted 3 May 2020

Abstract. The aim of this study is to investigate the morphological, functional group, crystallinity and mechanical properties of a three-dimensional porous cornstarch/n-HAp (nano-hydroxyapatite) biocomposite scaffold. In this study, cornstarch/n-HAp scaffolds were fabricated using the solvent casting and particulate leaching technique. The porous cornstarch/n-HAp composites with various cornstarch contents (30, 40, 50, 60, 70, 80 and 90 wt%) were prepared and characterized by scanning electron microscopy, Fourier transform infrared spectroscopy, X-ray diffractometer and compression test. The morphology of the scaffolds possessed macropores (200–600 μm) and micropores (50–100 μm) with a high interconnectivity. The porosity of the porous cornstarch/n-HAp scaffolds varied between 53 and 70% with compressive strength and compressive modulus of 2.03 and 8.27 MPa, respectively. The results suggested that highly porous cornstarch/n-HAp scaffold properties with adequate mechanical properties can be obtained for applications in bone tissue engineering.

Keywords. Scaffold; hydroxyapatite; mechanical; porous; starch.

1. Introduction

There is a high demand for alternative materials of human bones due to the increase of bone illnesses and longer life expectancy [1–3]. The development of manufactured materials is a major concern and requires assurance in supplanting bone tissues [4–6]. The alternative materials are expected to resemble the natural bone tissue. Hence, the manufactured material must be bioactive and possess resorbable properties, to enhance the host tissue regeneration and supplant the embedded material with newly implanted bone tissue [7–12].

As a potential bioceramic material, hydroxyapatites (HAp) (calcium phosphates) have been studied extensively for bone substitution in composite materials [13] due to their bioactivity, biocompatibility and osteoconductivity. These properties are used to describe capability in advanced cell proliferation, differentiation and adhesion [7,10]. However, HAp is brittle. Moreover, it is difficult to prepare HAp in complex forms as it does not possess the satisfactory features required for tissue engineering [1,7,13,14]. Thus, natural polymers, e.g., starch is crucial for use to improve the mechanical properties of HAp [3,15,16].

Starch is one of the essential polymers for medical applications because it is cost-effective, biodegradable, non-toxic and renewable. On the other hand, it can also act as an indispensable analogue polysaccharide to *in-vivo* energy storage that can metabolize into glucose [17–19]. In nature, plant polymers are biocompatible which can improve the bioactivity of ceramics [17,20]. Starch and HAp exhibit high biocompatibility. The fabricated scaffold using starch and HAp has reinforced mechanical properties and particular functionalities with sustainable features [21,22].

A temporary artificial extracellular matrix is applied to support functional tissue regeneration during scaffold fabrication. It is a challenge in tissue engineering [23–25]. The fabricated scaffold should have some essential features, i.e., great biocompatibility, appropriate biodegradation rate, minimal inflammatory activity, interconnected pore structure and adequate mechanical properties [10,26]. Also, the advantageous incorporation of bioactive molecules is an additional tissue substitute design requirement [27,28].

Starch granules contain both crystalline and amorphous components [29]. Starch has two macromolecules, i.e., amylose and amylopectin [30]. When starch is sufficiently heated in water, starch granules increase pressure on crystallites [30,31]. The granules collapse and lose contact with each other because the amylopectin backbones

Published online: 29 August 2020

extend in all directions [32]. Then, the double-stranded helices of amylopectin connect flexible spacer arms with amorphous clusters. The gelatinization phenomenon can be illustrated by the flexibility of the spacer arms [30–34]. The presence of amylose contributes to the amylopectin backbones in the amorphous lamellae, which reduces their flexibility and delays swelling [30,32,33,35]. The connected amylose and amylopectin can be evenly and effectively distributed into its tree-like structure across the granules. It can also transverse the HAp granules as an adhesive between the granules in order to form inter- and intra-hydrogen bonding among all the particles [36]. The process of retrogradation occurs when the amylose and amylopectin chains are rearranged and re-associated in a different ordered structure with a high level of crystallinity after cooling [30,33,34,37]. The HAp granule will be interlocked tightly in the recrystallization of macromolecule environment and this determines the structural hardness of the scaffold [30].

In this research study, a novel and hybrid three-dimensional (3D) porous cornstarch/n-HAp biocomposite scaffold was fabricated by utilizing the adhesion and recrystallization (due to output gelatinization and retrogradation, respectively) of starch without any additives to meet the requirements of a scaffold for bone regeneration. This method of fabrication is rapid with low energy consumption. It is also cost-efficient, simple and environmentally friendly. Many research studies have reported cornstarch-based scaffolds [38–45]. The highly porous biocomposite scaffold was prepared by the solvent casting and particulate leaching (SCPL) technique. The prepared sample was characterized using scanning electron microscopy (SEM), X-ray diffraction technique (XRD), Archimedes method, Fourier transform infrared (FTIR) spectroscopy and universal testing machine (UTM). The novel starch-based scaffold with outstanding mechanical properties and no detrimental effects was fabricated by controlling the rigorous preparation conditions, i.e., temperature and water content [30,46–48]. The pure green and natural 3D porous scaffolds based on starch have not been studied extensively. Many research studies have paid little attention to the tendency of natural starch which makes the scaffold highly porous and robust without crosslinking and coupling agents for the structural fabrication and enhancement when it is subjected to morphological change. Hence, a novel and hybrid scaffold has been fabricated which can provide the required characteristics.

2. Materials and methods

2.1 *Materials*

The 3D porous biocomposite scaffolds were fabricated by using cornstarch and hydroxyapatite nanopowder (n-HAp). Cornstarch, n-HAp and analytical grade sodium chloride (NaCl) particles porogen were commercially available. Ethanol (95%) was used as a water-repellent.

2.2 *Scaffold fabrication*

A 3D porous bioceramic scaffold was fabricated and reinforced by cornstarch to make it a biocomposite material. SCPL was implemented to prepare 3D porous cornstarch/n-HAp biocomposite scaffolds. The cornstarch was dissolved in deionized water (volume ratio of 1:3) to prepare a cornstarch suspension with a concentration of 333.33 g l^{-1}. Then, the cornstarch suspension was heated at temperature range within 45–65°C for about 30–60 min (heat-moisture treatment). To produce a composite scaffold which is made of cornstarch and n-HAp, the required weight of n-HAp (composition is listed in table 1) was dispersed in the cornstarch suspension through stirring using a vortex mixer at 3000 rpm for 1–3 min. Deionized water was added when the mass fraction of n-HAp and the cornstarch is >1. The volume of additional deionized water can be determined using the below equation:

$$V_{\mathrm{DI(Add)}} = V_{\mathrm{DI(starch)}} + 3\left(M_{\mathrm{HAp}} - M_{\mathrm{starch}}\right), \quad (1)$$

where $V_{\mathrm{DI(starch)}}$ is the initial volume of deionized water to obtain a cornstarch suspension; M_{HAp} is the mass of the n-HAp and M_{starch} is the mass of the cornstarch. The mixture was agitated and heated at a rate of 5°C min^{-1} for 10 min from 50 to 100°C. Subsequently, NaCl was added and stirred into the mixture to prepare a homogeneous composite. The ratio of NaCl to the total mass of cornstarch and n-HAp is 2:1. The NaCl–HAp–cornstarch homogeneous composite was filled into a Teflon mould and cooled within 2–10°C for about 1–2 h. Next, the homogeneous composite was dehydrated at a temperature range of 80–90°C for 20–24 h. Then, it was dried at 110–140°C for 2–3 h. The dried cornstarch composites were immersed in deionized water for 2–3 h for 15 min successively until the deionized water eliminated salt particles in the composites completely. The leached scaffolds were immersed into 95% ethanol for about 10–15 min for the sterilization and coacervation process. Lastly, the porous cornstarch/n-HAp scaffolds were dried at 85–95°C for 3–4 h and then stored in a desiccator before characterization.

2.3 *Scaffold characterization*

2.3a *Scanning electron microscope (SEM) analysis:* The morphology of the composite scaffolds was observed using an SEM. The prepared scaffold samples were sliced using a scalpel to reveal the cross-section of the samples. All the specimen slices were coated with a thin platinum (Pt) layer *via* sputtering. Subsequently, the coated samples were examined using an SEM at an acceleration voltage of 5 kV.

Table 1. Proportion of the cornstarch/n-HAp scaffolds.

Sample code	Starch (wt%)	n-HAp (wt%)	Cornstarch amount (g)	n-HAp amount (g)	NaCl amount (g)
HAp–Cs30	30	70	3	7	20
HAp–Cs40	40	60	4	6	20
HAp–Cs50	50	50	5	5	20
HAp–Cs60	60	40	6	4	20
HAp–Cs70	70	30	7	3	20
HAp–Cs80	80	20	8	2	20
HAp–Cs90	90	10	9	1	20

2.3b *Archimedes porosity determination (APD) analysis:* The porosity of the cornstarch/n-HAp scaffold was measured using the liquid displacement method based on the Archimedes principle. Three identical cuboid-shaped scaffolds were prepared for every different composition. The porosity of every scaffold representing each composition had to be calculated appropriately. The average porosity value of the three identical samples was calculated and used to determine the overall results. The porosity of each cornstarch/n-HAp scaffold was determined by using the following equation:

$$\text{Porosity} = \frac{(W_{\text{Saturated}} - W_{\text{Dry}})/p_{\text{ethanol}}}{(W_{\text{Saturated}} - W_{\text{Immersed}})/p_{\text{ethanol}}} \times 100\%, \quad (2)$$

where W_{Dry} is the weight of the dry specimen; $W_{\text{Saturated}}$ is the saturated weight of the specimen in ethanol; W_{Immersed} is the weight of the specimen immersed in ethanol and p_{ethanol} is the density of ethanol (0.798 g ml^{-1}).

2.3c *Fourier-transform infrared (FTIR) spectroscopy analysis:* The wavelength spectrum of the composite scaffolds was performed using a FTIR spectrometer. The prepared samples were ground into a fine powder using an aluminium oxide mortar and pestle to conduct the FTIR analysis. The cornstarch/n-HAp scaffold samples were analysed in transmission mode and collected over the frequency spectrum range of 600–4000 cm^{-1}.

2.3d *X-ray diffraction (XRD) analysis:* The crystallinity of the cornstarch/n-HAp biocomposites was investigated with an X-ray powder diffractometer. The prepared specimens were further ground into a fine powder using an aluminium oxide mortar and pestle to conduct the XRD analysis. The XRD operates with voltage and current settings of 40 kV and 30 mA, respectively, using Cu radiation (λ = 1.5406 Å). The graphical XRD patterns of the cornstarch/n-HAp biocomposites were determined using diffraction angles from 10 to 55° at a scan speed of 4° min^{-1} with the step size and step time of 0.02 and 0.24 s, respectively.

2.3e *Compressive property analysis:* The mechanical parameters of the composite scaffolds were measured by executing a compression strength test using the UTM. Cuboid-shaped scaffolds were prepared in 25 × 13 × 13 mm^3 for the compression tests. The compression tests were measured according to ASTM F 451-95 guidelines with the cross-head speed of 1 mm min^{-1} and 2 kN of load capacity. Three identical specimens for every composition were tested, and the average compressive strengths were recorded and reported. The slope for the initial linear portion of the stress–strain curve was plotted by using the test results to determine the compression modulus.

3. Results and discussion

3.1 *Morphological analysis*

SEM was used to examine the morphology of cornstarch/n-HAp scaffolds. SEM images of the scaffolds are important to analyse cross-sectional surface, average pore size and interconnectivity [49,50]. Meanwhile, APD analysis was used to elucidate the porosity percentage of cornstarch/n-HAp scaffolds. The variety of composite proportions resulted in different porosity, homogeneity, interconnectivity and pore size of the scaffold's inner structure [45,50].

The morphologies of the cornstarch/n-HAp scaffolds with varying cornstarch contents are shown in figure 1a–g. The average diameter of micropores and macropores for HAp–Cs30 are ~71 μm diameter and ~420 μm, respectively. Meanwhile, the average diameter of the HAp–Cs40 scaffold pores for micropores and macropores is ~97 μm and ~552 μm, respectively. HAp–Cs40 had a higher porosity percentage of 68.1% than the HAp–Cs30 scaffold with a porosity percentage of 61.6%. The HAp–Cs30 with a high HAp content has a 3D matrix with fewer pores (figure 1a) than HAp–Cs40 (figure 1b). The HAp–Cs50 scaffold has a good interconnection between the macroporous structure of pore size (~371 μm diameter) and micropores (~82 μm). The porosity was about 69.6% as listed in table 2. A decrease in the average pore size of the HAp–Cs50 leads to an increment of porosity due to the presence of the microcracks and highly dispersed pores. The rough and loose interior region of the matrix is formed (figure 1a–c) due to the subsequent increment of HAp

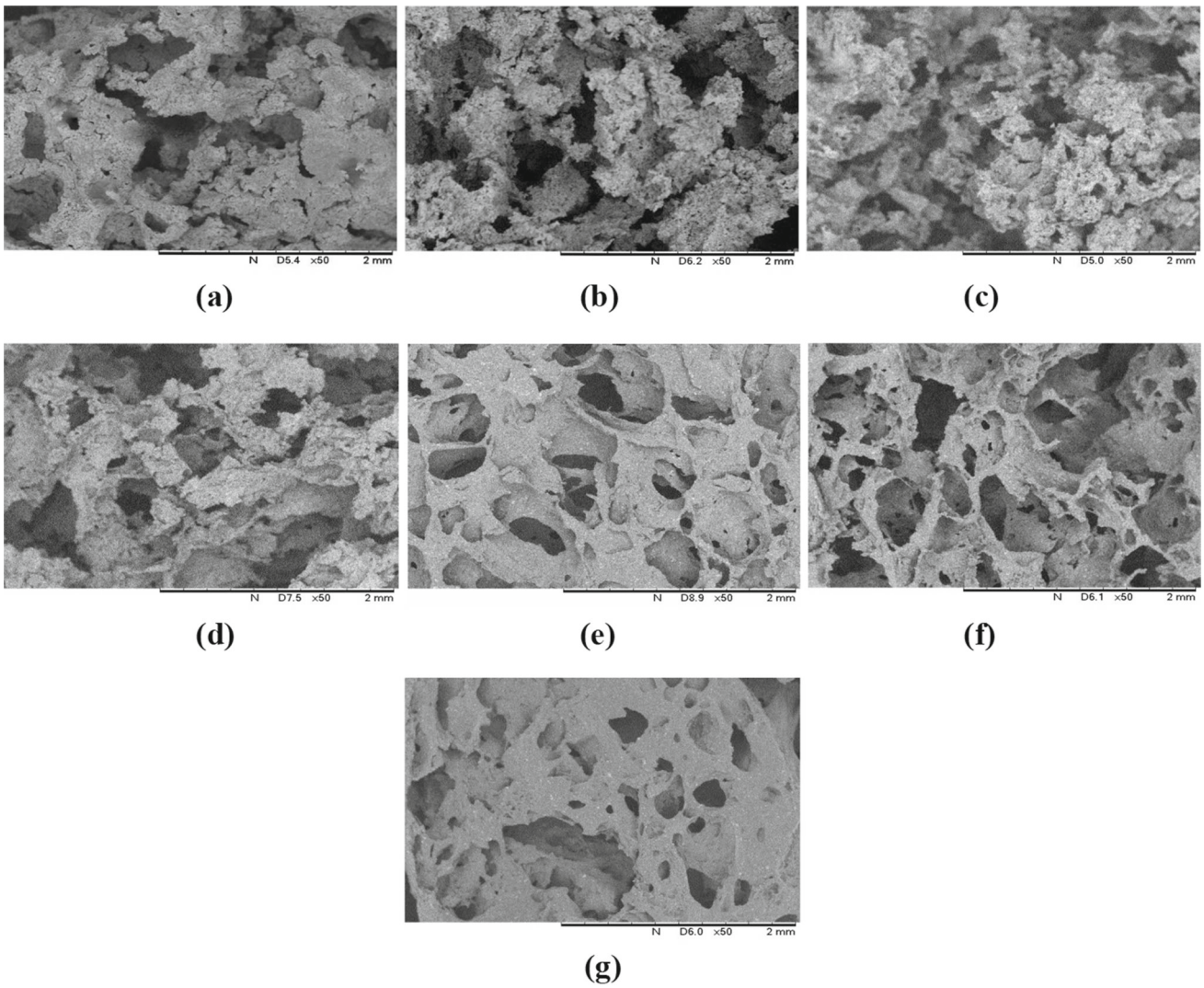

Figure 1. SEM images of 3D porous cornstarch/n-HAp scaffolds: (**a**) HAp–Cs30, (**b**) HAp–Cs40, (**c**) HAp–Cs50, (**d**) HAp–Cs60, (**e**) HAp–Cs70, (**f**) HAp–Cs80 and (**g**) HAp–Cs90.

concentration. It causes incomplete entrapment in the recrystallized cornstarch bed. Meanwhile, the porous structures are completely interconnected throughout the entire scaffold, even at low proportions of cornstarch. The cluster-like matrix structure of the scaffolds exhibits a higher porosity (more than 60%) and forms the porous microstructure with high interconnectivity, especially HAp–Cs50. The morphology of these irregular porous structures does not change significantly from a macroscopic point of view when cornstarch composition increases from 30 to 50 wt% (figure 1a–c).

The HAp–Cs60 scaffold was not so rigid and flaky with the lowest porosity (53%). Figure 1d shows highly interconnected open morphology of macropores with diameters around ∼478 μm and average micropore diameter of ∼87 μm. In contrast, figure 1d shows that HAp particles incorporated with recrystallized cornstarch walls of the pore and not in segmented clusters compared to those scaffolds in figure 1a–c. The HAp–Cs60 microarchitecture has the lowest porosity with a massive closed pore structure in the successive matrices of the scaffold. The average pore size of HAp–Cs70 (diameter of macropores ∼368 μm; diameter of

Table 2. Porosity and average pore size of the cornstarch/n-HAp scaffolds.

		Average pore size (μm)	
Sample	Porosity (%)	Micropores	Macropores
HAp–Cs30	61.6	71.4	419.8
HAp–Cs40	68.1	96.6	551.7
HAp–Cs50	69.6	81.7	371.2
HAp–Cs60	53.0	86.6	478.2
HAp–Cs70	58.2	62.2	368.3
HAp–Cs80	63.3	59.9	287.8
HAp–Cs90	61.6	52.2	291.3

micropores ~62 μm) is more significant than HAp–Cs80 (macropores, diameter ~288 μm; micropores, diameter ~60 μm). However, the HAp–Cs80 matrices had a higher porosity percentage of 63.3% than HAp–Cs70 scaffold with a porosity percentage of 58.2% due to a higher percentage of starch in composition. The decrement of average pore sizes in HAp–Cs70 and HAp–Cs80 structure that leads to high porosity is attributed to the homogeneous and well-interconnected structure. The smoother recrystallized layer of cornstarch is deposited on the walls of the interior region for the scaffold structure. The cornstarch covers the connecting areas between the pores or necklines of the connecting areas with high porosity. The overall network of interconnected pore architecture has been illustrated in the cross-sectional view from figure 1e and f. The pores of HAp–Cs80 are well distributed in the desired constitutive microstructure due to the contribution of the tiny round pores in the thin walls of the scaffolds, which are highly responsible for interconnectivity. In other words, the HAp–Cs70 can appreciate the typical network structure, which separates large pores with thick trabeculae. Meanwhile, the HAp–Cs80 struts are very thin, sintered well among adjacent pores, causes rough texture for strut and creates wide microporosity, which is an ideal cellular environment [50].

The suitable cornstarch content in composites can stabilize and enhance the formation of the porous scaffold structure. However, the HAp–Cs90 shows anomaly where its porosity decreases at the highest proportion of cornstarch content when compared to the scaffolds (cornstarch content percentage <90%) with a similar microstructural morphology, especially from figure 1d–f. Table 2 indicates that HAp–Cs90 shows lower porosity percentage (61.6%) than HAp–Cs80. It causes weak mechanical strength due to the collapsed structure. Insufficiency of HAp content proportion in the scaffold is the main factor that leads to this poor behaviour. On the other hand, the HAp–Cs90 has average macropore size diameter of ~291 μm. Besides, micropores with ~52 μm diameter are present in HAp–Cs90 and it is larger than HAp–Cs80. The HAp–Cs90 varies in matrix structure. Some regions in HAp–Cs90 are fragile, while others are ductile pores and they are not interconnected well. Deformation of pore size structures can be observed. It can be seen that HAp–Cs60, HAp–Cs70, HAp–Cs80 and HAp–Cs90 show a smoother surface of network structure (figure 1d–g) than HAp–Cs30, HAp–Cs40 and HAp–Cs50 where they exhibit a rough surface (figure 1a–c). HAp–Cs90 has thicker walls between pores than the HAp–Cs60, HAp–Cs70 and HAp–Cs80 scaffolds. The scaffold has low porous walls as seen from figure 1g. Composites with a high proportion of cornstarch content (HAp–Cs80 scaffolds with 80 wt% cornstarch and 20 wt% HAp) present the best structure, and it can be observed through figure 1f. HAp–Cs80 also has high porosity and stiffness when compared to other scaffolds.

The natural polymer cornstarch can be used in the formation of a scaffold in complex structures [51,52]. The structure and architecture of the pore-wall depend on the crystallizability and proportion of the cornstarch. The existence of pores is required for adequate neovascularization, nutrient transportation and removal of metabolic waste for cellular activities [51]. The pore size and porosity influence cell behaviour and determine the ultimate mechanical properties of the scaffold [44,53]. These morphological characteristics are required in bone tissue engineering because it is vital for cell colonization to ensure favourable *in-vitro* and *in-vivo* functionality [53].

3.2 *FTIR spectroscopy analysis*

FTIR spectroscopy was used to study the interactions of cornstarch/n-HAp for interpretation and evaluation of the functional groups and structural elements in the prepared samples. In the FTIR spectral pattern shown in figure 2, an identical pattern indicates that the scaffold samples were consistently fabricated. In the FTIR spectrum, it can find a significant peak of n-HAp and cornstarch appears throughout the spectrum with the wavelength range. Low peaks (weaker bands) are dispersed in the spectrum because the presence of cornstarch in the scaffold sample entraps n-HAp. Subsequently, it causes significant reflection and absorption of IR ray during the FTIR measurement. In other words, the transmittance would become insignificant. Hence, a weaker band is barely detected through FTIR.

Pure HAp presents a strong peak absorption FTIR band centred around 1000–1100 cm^{-1} due to asymmetric vibration stretching for phosphate ($–PO_4$) group [54,55]. It is evidence of the presence of HAp. The presence of weak board absorption peak bands (low and broad peak) in the region around 850–950 cm^{-1} was due to out-of-plane bending vibration stretching for carbonate ($–CO_3$) group of

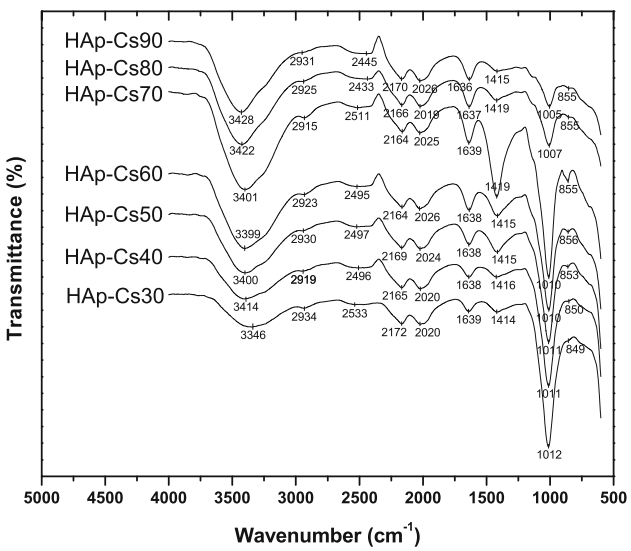

Figure 2. FTIR spectrum of 3D porous cornstarch/n-HAp scaffolds.

the HAp [56]. The functional group of carbonate exhibits at two peaks at different wavenumbers in the same band leading to the difference in stretching vibrational mode, i.e., asymmetric and out-of-plane vibration stretching. The peaks in the low-intensity transmittance region within 1400–1650 cm^{-1} are due to C–O asymmetric functional group $–CO_3$ [57–59]. A wide broad absorption band peak appearing within 3200–3600 cm^{-1} is due to symmetric stretching mode in functional groups O–H [57]. It is evidence to justify that the composite is HAp.

Characteristic broad bands of cornstarch in the 3100–3700 cm^{-1} refer to hydroxyl group (–OH) vibration stretching in the anhydroglucose unit. Meanwhile, characteristic broad bands of cornstarch in 2800–3000 cm^{-1} refer to the methylene(C–H) group vibration stretching in the glucose unit [60]. The weak board absorption peak bands $\sim$2485 cm^{-1} is due to C–H stretching vibration at the C-6 position of a glucose molecule [61]. Meanwhile, the peaks within 2000–2200 cm^{-1} are attributed to the O–H stretching vibration combination. It represents the degree of hydrogen bonding in the cornstarch. The adjacent peaks at the absorption band show that hydrogen links appear between amylose chains. Furthermore, this hydrogen link appears between amylose and amylopectin molecules too [62]. The peaks that present at $\sim$1638 cm^{-1} are attributed to the bending vibration stretching of O–H in the amorphous regions and asymmetric stretching in a carboxylate group (COO–) of cornstarch and it reveals that some amylopectin or amylose molecular chains found in cornstarch might be fragmented during fabrication [44,60,63]. The absorption at $\sim$1415 cm^{-1} is attributed to $–CH_2$ bending vibration and C–O–O stretching in a carbohydrate group [64]. The characteristic peaks at 800–1300 cm^{-1} are attributed to C–O–H bend stretching vibration, C–C stretching vibration and C–O stretching vibration of the glucose unit [65,66].

The absorption bands at 800–1300 cm^{-1} are sensitive to changes in the crystallinity of the cornstarch. The absorption band intensity at $\sim$1010 cm^{-1} determines the orientation of the –CH and $–CH_2$ intermolecular bond in the hydroxymethyl group ($–CH_2OH$) of cornstarch. The bands of 3100–3700, 2800–3000 and $\sim$1638 cm^{-1} are associated with retrogradation process of starch and recrystallization in the interactions of cornstarch/n-HAp composites [67]. As the cornstarch content of cornstarch/n-HAp composites increases, the increment of the intensity of peaks at the FTIR absorption bands might be able to illustrate the quantity of hydroxyl group (–OH) in cornstarch that interacts vigorously with HAp particles by interparticle, intraparticle and crystal bonding for the determination of mechanical properties of scaffolds. The increment of the proportion of the cornstarch and the crystallinity of composites are due to retrogradation. The retrogradation of cornstarch reduced the band absorption ratios and bandwidth for some peaks [66]. In comparison among the scaffold samples with different proportions, it can be noticed that the positions and shapes of the absorbance peaks on the FTIR spectra are slightly different. A comparative study on the variation of FTIR spectral pattern can be done to determine the extent of structural changes or composite crystallinity within the cornstarch/n-HAp scaffold to indicate the interaction with crystal nucleation [68].

3.3 *XRD analysis*

XRD techniques are commonly used for the phase identification of the crystalline material and the study of composite crystallinity demonstrates XRD patterns that exist among the cornstarch and HAp [21]. All natural starch contains long-range molecular structure regions and the common crystalline forms are commonly identified by XRD patterns as A, B and C. The crystallinity of A-type is most likely in cereal starch. The tubers and amylose-rich starches exhibit the B-type crystallinity. The C-type crystallinity is commonly found in legumes, a combination of A-type and B-type polymorphs. V-type crystallinity is also another crystalline form found in amylose which is integrated with monoglycerides and fatty acids into a complex form. In this case, V-type crystallinity occurs after starch gelatinization and retrogradation. V-type crystallinity is hardly found in natural starches [69]. However, limited literature is available to support and identify the V-type crystallinity complex accurately with characteristic diffracted peaks.

In this case, the XRD patterns of the cornstarch/n-HAp composites are within 10–55° for 2θ and shows noticeable and distinguishable peaks located at 2θ = 10.6, 15.1, 26, 29.1, 31.9, 39.8, 42.1, 49.5 and 53.3°. It suggests the recrystallization of the cornstarch as these peaks do not appear in the native starch in amylose and amylopectin. For the cornstarch/n-HAp composites, the sharp diffraction peaks at 2θ = 26, 29.1, 31.9 and 49.5° as shown in figure 3 are because of KCl face-centred cubic lattice in the recrystallized cornstarch [70,71]. As the crystalline structure of natural cornstarch granules vanishes during the fabrication of porous scaffolds, the retrograded cornstarch exhibits a typical crystalline V-type structure. Similarly, the peaks at 2θ = 26, 29.1 and 31.9° seem more apparent and obvious as the cornstarch content increases [71]. The intensities of these peaks increase when the cornstarch content in the cornstarch/n-HAp composites increases. Each peak intensity is composed of a different combination of phase combination which is proportional to the crystalline concentration.

The composites from 10 to 70 wt% of HAp content exhibit indistinct characteristic peaks of HAp. It indicates that the highly pure crystalline phase of HAp is maintained due to the fabrication of scaffold at low temperature. The peak profile of HAp is widely exhibited due to nanocrystallites and significant lattice disorder that does not significantly increase the crystallinity of the HAp particles [72]. In other words, the cornstarch/n-HAp composite with the

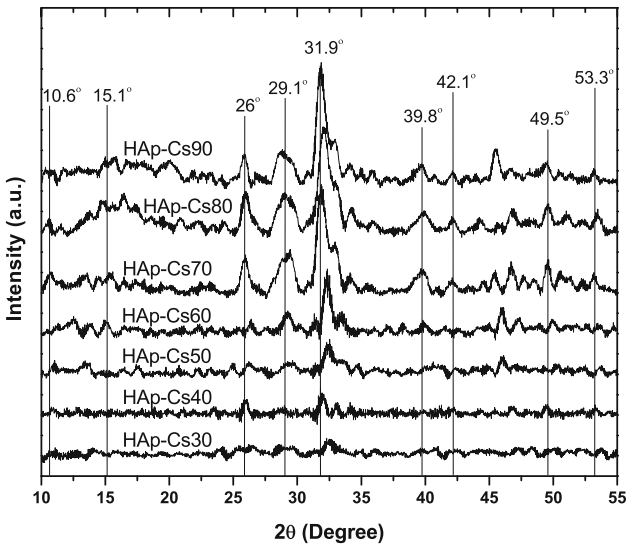

Figure 3. XRD spectrum of 3D porous cornstarch/n-HAp scaffolds.

decrement of cornstarch content presents a broad line of peak and these peaks overlap in the XRD patterns. It indicates that the higher proportion of HAp crystals has a smaller size and lower crystallinity. This is because HAp particles are not sintered when the fabrication procedure is conducted at low temperature [73]. However, the XRD patterns of the cornstarch/n-HAp composites seem consistent with the diffraction peaks of stoichiometric HAp when the cornstarch content increases. The similarity of the XRD patterns might be due to the interaction between the cornstarch and HAp; the HAp particles are trapped in the recrystallized cornstarch matrix. Thus, the HAp particles that coat the cornstarch crystalline structure exhibit a similar pattern as the highly crystalline HAp-like structure in the XRD patterns.

In figure 3, the peaks in the XRD patterns can be used to illustrate the interaction among the cornstarch/n-HAp composites. When the cornstarch content increases, the crystallinity of cornstarch/n-HAp composites can be increased through the process of recrystallization. This process can cause stiffness in the composites. The cornstarch/n-HAp composites with the higher intensity of the characteristic peaks in the XRD patterns have a higher degree of crystallinity.

3.4 *Compressive property analysis*

Compressive properties are essential in designing bone tissue scaffolds to present the desirable mechanical properties of the injured bone tissue for the regeneration of bone tissue [49]. The compressive strength and modulus can be used to infer functions of the crystalline phase and internal geometry of the scaffolds [74]. The composites' compression strength and module were measured through the compression test. Compressive properties of all seven scaffold samples with various cornstarch contents are listed in table 3. The mechanical properties of the HAp (composite) are enhanced by the presence of the cornstarch in the matrix. Homogeneously, the compressive strength and modulus for the porous 3D HAp samples increase in proportion to the addition of starch [36].

Table 3. Mechanical properties of the cornstarch/n-HAp scaffolds.

Sample	Compressive strength (MPa)	Compressive modulus (MPa)
HAp–Cs30	0.031 ± 0.002	0.3343 ± 0.011
HAp–Cs40	0.070 ± 0.001	0.6185 ± 0.004
HAp–Cs50	0.231 ± 0.003	2.8939 ± 0.030
HAp–Cs60	0.645 ± 0.006	4.3638 ± 0.090
HAp–Cs70	1.222 ± 0.003	7.4178 ± 0.074
HAp–Cs80	2.031 ± 0.014	8.2723 ± 0.093
HAp–Cs90	1.237 ± 0.003	7.7942 ± 0.047

The highest compressive strength can be observed for HAp–Cs80 (2.031 ± 0.014 MPa). Meanwhile, the scaffold sample with the lowest compressive strength is HAp–Cs30 (0.031 ± 0.002 MPa). The compressive strength increases with the increment of cornstarch content. A similar trend in the compressive modulus of the cornstarch/n-HAp scaffolds can be observed too in table 3. The HAp–Cs80 scaffolds (80 wt% cornstarch content) achieved a maximum compressive module of 8.2723 ± 0.093 MPa which is 25 times the compressive modulus of the HAp–Cs30 scaffolds (0.3343 ± 0.011 MPa). Likewise, the addition of cornstarch can significantly increase the compressive modulus of the scaffolds. The compressive strength and modulus of scaffolds are significantly increased by multiples of 2 and 3, respectively, when the cornstarch content increases from 40 to 50 wt%. It is due to the binding effect of the cornstarch. This finding can be used to infer the porosity of cornstarch/n-HAp composites, which has sufficient content of cornstarch. The adequate adhesive interactions between the HAp particles are due to the adhesive force of cornstarch. Likewise, a significant improvement in the compressive strength and modulus of the HAp–Cs70 can be observed due to the adhesive effect, where the compressive strength and modulus double for HAp–Cs60 when cornstarch content increases from 60 to 70 wt%. When the quantity of cornstarch granules is high, the gelatinized molecular chains can be extended substantially and penetrate the space among the HAp particles. Association among the particles could lead to the reinforcement of interior architecture of the cornstarch/n-HAp scaffold [36]. However, the compression strength decreases from 2.031 ± 0.014 to 1.237 ± 0.003 MPa when the cornstarch content increases from 80 to 90 wt%. The compression modulus also

decreases from 8.2723 ± 0.093 to 7.7942 ± 0.047 MPa as the cornstarch content increases from 80 to 90 wt%. Both decrements might occur due to severe shrinkage of scaffolds. A further decrement of HAp content will lead to the loss of structural rigidity due to insufficiency of HAp. Inadequate HAp content hinders reaction of the cornstarch with HAp particles in interlocking affecting the compressive strength and modulus of the scaffolds [44].

In the literature [75] and [76], the measured compressive strength and modulus values of human cancellous bone vary from 0.22 to 10.44 MPa and 1 to 9800 MPa, respectively. The human bone mechanical properties are attributed to various physiological factors [75,76]. In this research study, the HAp–Cs80 scaffolds show the most suitable mechanical properties among all the cornstarch/n-HAp scaffolds that are highly similar to human cancellous bone. The HAp–Cs80 scaffold has the typical compressive strength and modulus. It indicates that the mechanism of reinforcement occurs between HAp and cornstarch during recrystallization. These porous cornstarch/n-HAp composites, therefore, have high potential in the regeneration of bone tissue cells and the cultivation of extracellular matrix with adequate mechanical properties in implantation of a bone scaffold.

4. Conclusions

Cornstarch/n-HAp biocomposite scaffolds were fabricated *via* SCPL to produce highly porous 3D scaffolds. In this study, the effect of cornstarch/n-HAp proportion on the microstructure, crystallinity and mechanical properties of the scaffold were studied. When the cornstarch content increases, the cornstarch/n-HAp scaffold will exhibit significant porosity, optimum pore size, high crystallinity, excellent pore interconnection and adequate mechanical properties that can be seen *via* the results of this study. These characteristics are essential in the application of bone tissue engineering. The scaffold fabrication technique without chemical additives can be used for the fabrication of green biocomposite scaffolds for potential use in bone tissue engineering applications. The properties of the fabricated composite scaffolds in this study meet the requirement when a suitable proportion of both HAp and cornstarch content is found.

Acknowledgements

We wish to thank Universiti Malaysia Perlis for providing material and facilities for this research. We would like to acknowledge the support from the Fundamental Research Grant Scheme (FRGS) under a grant number of RACER/1/2019/STG07/UNIMAP/2 from the Ministry of Higher Education Malaysia.

References

[1] Ficai D, Ficai A, Melinescu A and Andronescu E 2017 *Nanostructures for cancer therapy* (Netherland: Elsevier)
[2] Lyles M B, Hu J C, Varanasi V G, Hollinger J O and Athanasiou K A 2015 *Regenerative engineering of musculoskeletal tissues and interfaces* (Netherland: Elsevier)
[3] Yunus Basha R, Sampath S K and Doble M 2015 *Mater. Sci. Eng. C* **57** 452
[4] Sheikh Z, Najeeb S, Khurshid Z, Verma V, Rashid H and Glogauer M 2015 *Materials (Basel)* **8** 5744
[5] Egol K A, Nauth A, Lee M, Pape H C, Watson J T and Borrelli J 2015 *J. Orthop. Trauma* **29** S10
[6] Shrivats A R, McDermott M C and Hollinger J O 2014 *Drug Discov. Today* **19** 781
[7] Ramesh N, Moratti S C and Dias G J 2018 *J. Biomed. Mater. Res. Part B* **106** 2046
[8] Khan A F, Saleem M, Afzal A, Ali A, Khan A and Khan A R 2014 *Mater. Sci. Eng. C* **35** 245
[9] Gong T, Xie J, Liao J, Zhang T, Lin S and Lin Y 2015 *Bone Res.* **3** 15029
[10] Pina S, Oliveira J M and Reis R L 2015 *Adv. Mater.* **27** 1143
[11] Farhat W and Drake J (eds) 2015 *Bioengineering for surgery in the critical engineer surgeon interface* 1st edn (Netherland: Elsevier)
[12] Jazayeri H E, Tahriri M, Razavi M, Khoshroo K, Fahimipour F, Dashtimoghadam E *et al* 2017 *Mater. Sci. Eng. C* **70** 913
[13] Habraken W, Habibovic P, Epple M and Bohner M 2016 *Mater. Today* **19** 69
[14] Kumar A, Biswas K and Basu B 2015 *J. Biomed. Mater. Res. Part A* **103** 791
[15] Sharma C, Dinda A K, Potdar P D, Chou C F and Mishra N C 2016 *Mater. Sci. Eng. C* **64** 416
[16] Chung J H, Kim Y K, Kim K H, Kwon T Y, Vaezmomeni S Z, Samiei M *et al* 2016 *Nanomed. Biotechnol.* **44** 277
[17] Roslan M R, Nasir N F M, Cheng E M and Amin N A M 2016 In: *International conference on electrical electronics, and optimization techniques* 2016 p 1857
[18] Makhijani K, Kumar R and Sharma S K 2015 *Crit. Rev. Environ. Sci. Technol.* **45** 1801
[19] Bin Park S, Lih E, Park K S, Joung Y K and Han D K 2017 *Prog. Polym. Sci.* **68** 77
[20] Nourmohammadi J, Ghaee A and Liavali S H 2016 *Carbohydr. Polym.* **138** 172
[21] Miculescu F, Maidaniuc A, Miculescu M, Dan Batalu N, Cătălin Ciocoiu R, Voicu Ş I *et al* 2018 *ACS Omega* **3** 1338
[22] Shakir M, Jolly R, Khan M S, Iram N E and Khan H M 2015 *Int. J. Biol. Macromol.* **80** 282
[23] Khorshidi S, Solouk A, Mirzadeh H, Mazinani S, Lagaron J M, Sharifi S *et al* 2015 *J. Tissue Eng. Regener. Med.* **10** 715
[24] Cheng A, Schwartz Z, Kahn A, Li X, Shao Z, Sun M *et al* 2018 *Tissue Eng. Part B* **25** 14
[25] Tang D, Tare R S, Yang L Y, Williams D F, Ou K L and Oreffo R O C 2016 *Biomaterials* **83** 363
[26] Wang X, Xu S, Zhou S, Xu W, Leary M, Choong P *et al* 2016 *Biomaterials* **83** 127
[27] Ho-Shui-Ling A, Bolander J, Rustom L E, Johnson A W, Luyten F P and Picart C 2018 *Biomaterials* **180** 143
[28] Guo B, Lei B, Li P and Ma P X 2015 *Regen. Biomater.* **2** 47

[29] Eliasson A C (ed) 2017 *Carbohydrates food* (Boca Raton: CRC Press)
[30] Wang S, Li C, Copeland L, Niu Q and Wang S 2015 *Compr. Rev. Food Sci. Food Saf.* **14** 568
[31] Yang Z, Gu Q, Lam E, Tian F, Chaieb S and Hemar Y 2016 *Food Hydrocolloids* **56** 58
[32] Bertoft E 2017 *Agronomy* **7** 56
[33] Nakamura Y 2015 *Starch: metabolism and structure* (Japan: Springer)
[34] Vamadevan V and Bertoft E 2018 *Food Hydrocolloids* **80** 88
[35] Zhang C, Han J A and Lim S T 2018 *Food Hydrocolloids* **77** 894
[36] Ahmed Y M Z, Ewais E M M and El-Sheikh S M 2015 *J. Asian Ceram. Soc.* **3** 108
[37] Fu Z, Chen J, Luo S J, Liu C M and Liu W 2014 *Starch/Starke* **67** 69
[38] Mohd Hori N A F, Mohd Nasir N F, Mohd N A, Cheng E M and Sohaimi S N 2017 In *IEEE-EMBS Conf. Biomed. Eng. Sci.,* Kuala Lumpur, Malaysia p 220
[39] Arafat M T, Gibson I and Li X 2014 *Rapid Prototypying J.* **20** 13
[40] Ali Akbari Ghavimi S, Ebrahimzadeh M H, Shokrgozar M A, Solati-Hashjin M and Abu Osman N A 2015 *Polym. Test.* **43** 94
[41] Velasquez D, Pavon-Djavid G, Chaunier L, Meddahi-Pellé A and Lourdin D 2015 *Carbohydr. Polym.* **124** 180
[42] Nasri-Nasrabadi B, Mehrasa M, Rafienia M, Bonakdar S, Behzad T and Gavanji S 2014 *Carbohydr. Polym.* **108** https://doi.org/10.1016/j.carbpol.2014.02.075
[43] Hadisi Z, Nourmohammadi J and Mohammadi J 2015 *Ceram. Int.* **41** 10745
[44] Koski C, Onuike B, Bandyopadhyay A and Bose S 2018 *Addit. Manuf.* **24** 47
[45] Roslan M R, Nasir N F M, Cheng E M and Mamat N 2016 In *International conference of electrical and electronic optimum technology* (Chennai: IEEE) p 1560
[46] Ai Y and Jane J L 2015 *Starch/Starke* **67** 213
[47] Ashogbon A O and Akintayo E T 2014 *Starch/Starke* **66** 41
[48] Kong X, Zhu P, Sui Z and Bao J 2015 *Food Chem.* **172** 433
[49] Bose S, Roy M and Bandyopadhyay A 2012 *Trends Biotechnol.* **30** 546
[50] Hutmacher D W 2006 *Biomaterials* **21** 175
[51] Bose S and Bandyopadhyay A 2016 In *Materials devices bone disorders* S V Gohil, S Suhail, J Rose, T Vella and L S Nair (eds) (Massachusetts: Academic Press) p 349
[52] Talou M, Miranzo P and Camerucci M A 2017 *Int. J. Appl. Ceram. Technol.* **14** 738
[53] Kim S S, Sun Park M, Jeon O, Yong Choi C and Kim B S 2005 *Biomaterials* **27** 1399
[54] Rocha J H G, Lemos A F, Kannan S, Agathopoulos S and Ferreira J M F 2005 *J. Mater. Chem.* **15** 5007
[55] Mobasherpour I, Heshajin M S, Kazemzadeh A and Zakeri M 2007 *J. Alloys Compd.* **430** 330
[56] Sato M, Wada M, Miyoshi N, Imamura Y, Noriki S, Uchida K *et al* 2004 *Acta Histochem. Cytochem.* **37** 101
[57] Li B, Chen X, Guo B, Wang X, Fan H and Zhang X 2009 *Acta Biomater.* **5** 134
[58] Meejoo S, Maneeprakorn W and Winotai P 2006 *Thermochim. Acta* **447** 115
[59] Siriphannon P, Kameshima Y and Yasumori A 2002 *J. Eur. Ceram. Soc.* **22** 511
[60] Ma Z and Boye J I 2017 *Crit. Rev. Food Sci. Nutr.* **58** 1059
[61] Lian X, Zhang K, Luo Q, Wang C and Liu X 2012 *Int. J. Biol. Macromol.* **50** 119
[62] Judawisastra H, Sitohang R D R, Marta L and Mardiyati 2017 In *Materials science and engineering conference series* vol 223 p 012066
[63] Soliman E A and Furuta M 2014 *Food Nutr. Sci.* **5** 1040
[64] Jiang S, Yu Z, Hu H, Lv J, Wang H and Jiang S 2017 *LWT* **84** 10
[65] Li G, Zeng J, Gao H, Li X, Li G, Zeng J *et al* 2011 *Int. J. Food Prop.* **14** 978
[66] Van Soest J J G, Tournois H, De Wit D and Vliegenthart J F G 1995 *Carbohydr. Res.* **279** 201
[67] Flores-Morales A, Jiménez-Estrada M and Mora-Escobedo R 2012 *Carbohydr. Polym.* **87** 61
[68] Sadjadi M S, Meskinfam M and Jazdarreh H 2010 *Int. J. Nano Dimens.* **1** 57
[69] Rodriguez-Garcia B, Londoño-Restrepo M E, Ramirez-Gutierrez S M and Millan-Malo C F (eds) 2018 *Effect of the crystal size on the X-ray diffraction patterns of isolated starches* (New York: Cornell University)
[70] Song Y and Jane J 2000 *Carbohydr. Polym.* **41** 365
[71] Lian X, Cheng K, Wang D, Zhu W and Wang X 2018 *Int. J. Food Prop.* **20** S3224
[72] Zanotto A, Saladino M L, Martino D C and Caponetti E 2012 *Adv. Nanopart.* **1** 21
[73] Li J, Liu X, Zhang J, Zhang Y, Han Y, Hu J *et al* 2012 *Appl. Biomater.* **100** 896
[74] Sabree I, Gough J E and Derby B 2015 *Ceram. Int.* **41** 8425
[75] Lakatos É, Magyar L and Bojtár I 2014 *J. Med. Eng.* **2014** 470539
[76] Rider P, Kačarević Ž P, Alkildani S, Retnasingh S, Schnettler R and Barbeck M 2018 *Int. J. Mol. Sci.* **19** pii: E3308